Journal of the Earth and Space Physics
Homepage: https://jesphys.ut.ac.ir
Vol. 51, No. 4, Winter 2026, P. 167-188
(Research Article)

Flood Risk Spatial Analysis via Integrating SCS-CN and Logistic Regression Methods (Case Study: Kalateh-ye Qanbar Drainage Basin in Nishabur)

Naemitabar, M.[1] ✉ | Zangeneh Asadi, M. A.[1] | Goli Mokhtari, L.[1]

1. Department of Climatology and Geomorphology, Faculty of Geography and Environmental Science, Hakim Sabzevari University, Sabzevar, Iran.

Corresponding Author E-mail: mahnaznaemi70@gmail.com

(Received: 8 Sep 2025, Revised: 15 Nov 2025, Accepted: 5 Jan 2026, Published online: 17 March 2026)

Abstract

Flood-prone area analysis within drainage basins plays a crucial role in flood risk management and planning. This study evaluated the performance of the Logistic Regression (LR) model and the Soil Conservation Service–Curve Number (SCS-CN) method for flood forecasting and zoning. A total of 17 criteria were incorporated, including elevation, slope, aspect, plan and profile curvature, precipitation, drainage density, distance to rivers, lithology, land use/cover, soil type, Normalized Difference Vegetation Index (NDVI), Slope Length Factor (SLF), Stream Power Index (SPI), Topographic Position Index (TPI), Terrain Roughness Index (TRI), and Topographic Wetness Index (TWI). In the SCS-CN model, groundwater infiltration (S) and surface runoff (Q) were estimated, while the Analytical Hierarchy Process (AHP) was applied to assign weights to the factors. Flood hazard maps for 5, 15, 25, and 50-year return periods were then generated based on weighted layers. The Receiver Operating Characteristic (ROC) curve was used to validate zoning results against the LR model. Findings indicated that the CN model outperformed LR, achieving RMSE = 0.143, MSE = 0.021, AUC = 0.921, and STD = 0.311. Within the LR model, lithology, proximity to rivers, and NDVI were the most influential predictors, while in the CN model, aspect, drainage density, precipitation, and land use were also dominant factors. Results further showed that 45–50% of the basin could be classified as having medium to high flood potential over the 5 to 50-year periods, particularly in downstream reaches and riverbeds. Given the concentration of settlements and agricultural activities, these areas represent critical zones for flood crisis management and mitigation.

Keywords: Flood, Zoning, CN model, ROC curve, Logistic regression, Risk.

1. Introduction

Since the beginning of life on earth, drought, and flood have affected human activities worldwide. Flood plains are a vital ecological part of arid and semi-arid regions, which, with fertile soil and water flow, are considered an important hub for agriculture and human habitation. However, occasional river floods constantly threaten these ecologically vulnerable areas and cause irreparable financial and human losses (Rustaei et al., 2020). Floods occur due to a sudden rise in river water levels due to snowmelt or heavy precipitation (Darabi et al., 2021). Floods cause casualties and economic losses in agricultural and urban areas, which is particularly important for this reason (Panahi et al., 2021; Ahmadlou et al., 2019). Floods are often recurring natural phenomena that affect the global community regardless of their geographic location or socio-economic development, as shown by data collected by the International Natural Disaster Database for the years 1900- 2020 is evident (Garrote, 2022). Flood risk increases in low-lying and low-lying areas (Fang et al., 2022). Climate change especially leads to an increase in the intensity and frequency of torrential rains, which is the main cause of flood intensification (Prein et al., 2017; Nachappa et al., 2020; Tabari, 2020). Various hydrological models have been developed and widely used in the past decades for flood forecasting (Crawford, 1699; Zhao et al., 1995). However, accurate prediction of flood-prone areas is difficult, mainly due to floods' complex and dynamic nature (Hong et al., 2018; Kia et al., 2012; Rozalis et al., 2010). Several local-scale and global-scale methods for accurate flood risk assessment have been developed based on traditional

Cite this article: Naemitabar, M., Zangeneh Asadi, M. A., & Goli Mokhtari, L., (2026). Flood Risk Spatial Analysis via Integrating SCS-CN and Logistic Regression Methods (Case Study: Kalateh-ye Qanbar Drainage Basin in Nishabur). *Journal of the Earth and Space Physics*, 51(4), 167-188. DOI: http//doi.org/10.22059/jesphys.2026.401169.1007717

E-mail: (1) ma.zanganehasadi@hsu.ac.ir | l.mokhtari@hsu.ac.ir

Publisher: University of Tehran Press.
DOI: http//doi.org/10.22059/jesphys.2026.401169.1007717
Print ISSN: 2538-371X
Online ISSN: 2538-3906

hydrological and hydraulic models (Bates et al., 2010; Yamazaki et al., 2011; Pappenberger et al., 2012; Winsemius et al., 2013; Rudari et al., 2015; Sampson et al., 2015; Dottori et al., 2016; Schumann et al., 2016). Flood forecasting models include machine learning methods that yield better results compared to other flood sensitivity assessment approaches although their performance differs from the algorithm employed (Wang et al., 2019). Machine learning algorithms are easy to implement (fast training, testing, and validation) and have very low computational costs. It is also less complicated than other physical and conventional models (Mekanik et al., 2013; Mosavi et al., 2017). Therefore, using flood mitigation methods is considered the best strategy for flood risk management (Khosravi et al., 2019; Tien Bui et al., 2017). Many researchers have used several methods to develop flood susceptibility models. Many researchers have used several methods to develop flood-prone models (Sahana et al., 2020; Costache and Bui, 2020). In recent years, numerous studies have investigated the effectiveness of machine learning algorithms in flood forecasting. These studies, which have used a variety of methods, including artificial neural networks, decision trees, and hybrid models, have shown that machine learning can significantly improve forecast accuracy. This growing trend in the use of intelligent methods indicates a paradigm shift in hydrological modeling, including machine learning algorithms (Bui et al., 2019; Wang et al., 2019; Wang et al., 2020; Shahabi et al., 2020; Dodangeh et al., 2020, Sulaiman and Wahab, 2017; Zhao et al., 2018, Samanta et al., 2018; Khosravi et al., 2019; Tehrany and Kumar, 2018 , Pradhan, 2010; Lee et al., 2018; Tehrany et al., 2019; Wubalem et al., 2021; El-Rawy et al., 2022, Aditian et al., 2018; Polykretis et al., 2018; Soma et al., 2019, Nguyen et al., 2017; Sahana et al., 2020, Lyu et al., 2020; Santos et al., 2019; Tang et al., 2018, Aziza Abbas et al., 2014; He et al., 2019; Jehanzaib et al., 2022; Cai and Xu, 2022; Hosein et al., 2022; Shatnawi and Ibrahim, 2022; Upretia and Ojha, 2022, Xu et al., 2024; Linusa et al., 2024; Pavesi et al., 2024; Hitouri et al., 2024; Gholami et al., 2025; Obada et al., 2025, Islam et al., 2025). Numerous studies have shown that machine learning and deep learning algorithms have played an essential role in improving the accuracy of flood risk zoning. A significant part of these studies has used classical machine learning methods, such as decision trees, random forests, support vector machines, and Bayesian methods, to predict floods. Another group of researchers has sought to better identify the complex, nonlinear relationships between environmental factors and flood events by using neural networks, hybrid models, and feature selection methods. More recent studies have also used deeper models, attention mechanisms, and explainability methods, such as SHAP, to enhance the accuracy, transparency, and reliability of results. Overall, these studies show that the use of machine learning methods can produce flood susceptibility and risk maps with higher accuracy and can be very effective in management decision-making. This study aims to investigate the risk of flooding in the Kalateh-ye Qanbar Drainage Basin in Nishabur. Considering the region's large size and the prevalence of dry and semi-arid climatic conditions, it is possible to understand the importance of flood risk assessment and zoning in this basin. This issue is especially important due to the vast agricultural lands and the protection of water and soil resources. Also, the current research is the development of modeling using the Curve Number (CN) model with the help of geomorphic factors and comparing its performance with the regression model to compare the models and determine the relative advantage of these two models in flood forecasting. Therefore, flood risk zoning in the study drainage basin is one of the basic steps in the management measures related to reducing and dealing with flood risk.

2. Material and Methods

2-1. Study area

Covering an area of 2,422.2 hectares in the southeast of Nishabur city, Zabarkhan and Mianjolgeh districts, Kalateh-ye Qanbar Drainage Basin is located at a distance of about 55 kilometers to the southeast of Nishabur city at latitude: 53°58'58" E and longitude: 53°49'35" N. Also, some areas are located in Kadkan District, north of Torbat-e Heydariyeh city. This area is part of the central Iran zone. Generally, the geology of

this area is formed from the erodible rocks of the Neogene, which is a part of the third era of geology. Another characteristic of this basin is the presence of high-density waterways in them, which cause muddy floods (Figure 1). The study area has significant topographic irregularities that is located in a mountainous region with outcrops of metamorphic rocks, including the ophiolite complex and Jurassic granites. Lower Cambrian rocks and the Chah Palang Formation also outcrop in this area, indicating a complex geological and topographic diversity. In terms of land cover and use, studies show that land use and land surface cover in similar regions of Iran have undergone significant changes under the influence of natural and human factors, making these layers important factors in erosion and environmental models. In terms of climate, the average annual rainfall in neighboring areas, such as Sabzevar, has a coefficient of variation of about 34.3%, and the primary precipitation season is winter. The average annual temperature has also been increasing, with a coefficient of variation of 97.5%, indicating significant temperature fluctuations in the region (Taheri and Ahmad, 2012).

2-2. Methodology

In the current research, the area's height was determined digitally using the DEM digital height model in Arc GIS 10/4 software to check the flood situation in the study area. Sentinel-2 satellite images of 2022 were used to prepare the land use map. Equation (1) for preparing the TWI and SPI maps is obtained from Equation (2). Next, 30-year data (2004-2024) were used to prepare the precipitation layer. Then, the kriging interpolation method was employed to prepare the precipitation map because this method has the lowest error value of root mean square error (RMSE) and absolute mean error (MEA). Equation (3) was used to prepare the vegetation density layer. The maximum infiltration map in the region is obtained using Equation (4). This layer shows the amount of rain that infiltrates the earth's surface. In the next step, precipitation zones with 5, 15, 25, and 50 years return periods were prepared from the data related to the maximum daily precipitation (29 meteorological stations with a standard statistical period of 30 years). Then they were interpolated using the Inverse Distance Weighted (IDW) model. Since the smallest error in the precipitation data was type II, Equation (5) was used to plot the runoff layer. The dataset is illustrated in Table 1. The flowchart of the research steps is shown in Figure 2.

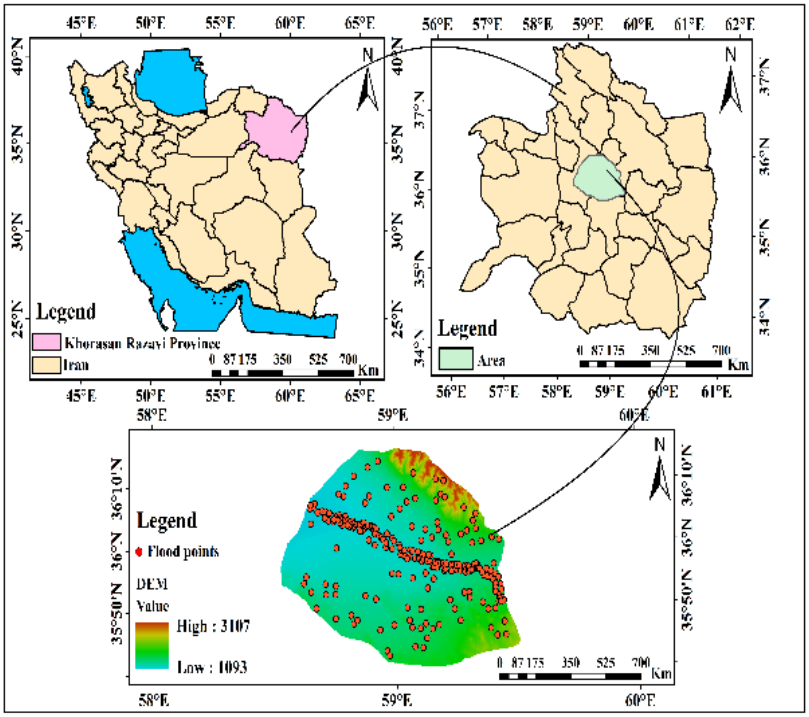

Figure 1. Geographical location of the study area.

Table 1. The parameters used to prepare the flood sensitivity map.

Parameters	Sources of data extraction	data type	Scale
Slope	Topography map	Vector	1:50000
DEM	ASTER sensor	Grid	30×30
Lithology	Geological map	Vector	1:100000
CN map	Natural and urban land use map (Khorasan Razavi Natural Resources Organization), soil map (Khorasan Razavi Watershed Organization), and Landsat 8 satellite images (USGS website)	Grid	12.5 Meter
Rainfall	Statistical hydrological and climatic data of rain gauge stations	Grid	30×30
Runoff coefficient	Topography map	Vector	1:50000
Land use	Natural and urban land use map (Khorasan Razavi Natural Resources Organization)	Vector	1: 100000
Elevation	DEM	Grid	12.5 Meter
NDVI	Landsat 8 satellite images (USGS website)	Grid	30×30
TWI, SPI,TRI, SLF, TPI	Aster sensor	Grid	30×30

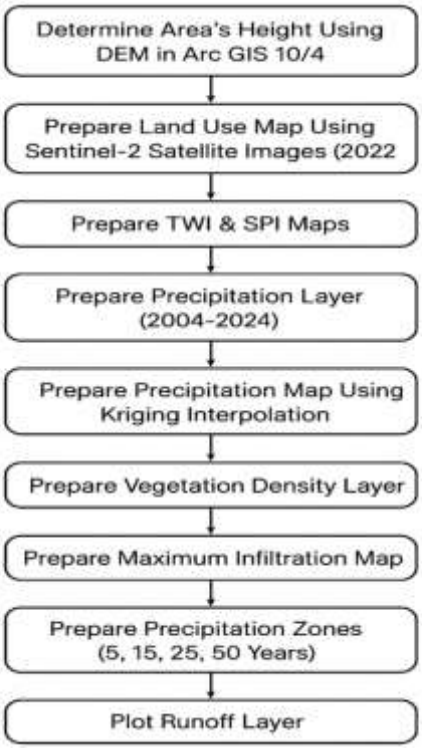

Figure 2. Flowchart of research steps.

2-3. The US Soil Conservation Service (SCS) method

The US Soil Conservation Service (SCS) method is widely used to estimate runoff based on rainfall and basin characteristics, particularly in watersheds where direct runoff measurements are unavailable (Mohammadi and Panahi, 2006; Abedini & Lotfi, 2019). Runoff is a critical component of surface water hydrology.

In this study, the maximum 24-hour precipitation data from meteorological stations over a 30-year statistical period were used to estimate the runoff height. The SCS method calculates the runoff using Equation (1):

$$Q = \frac{(P-0.2)^2}{(P+0.8S)^2} \quad \text{for} \quad SP > 0.2 \qquad (1)$$

where: Q is the runoff height (mm),
P is the 24-hour precipitation height (mm)

S represents the maximum storage capacity related to interception, infiltration, and surface storage (Mahdavi, 2023).
The parameter SSS is influenced by land cover type, land use, and soil permeability. It is derived from the dimensionless Curve Number (CN), which ranges from 0 to 100. A CN value of 0 indicates no runoff generation from precipitation, while a CN value of 100 implies that all rainfall becomes surface runoff, making runoff height equal to precipitation height (Hawkins, 1980).

2-4. Topographic wetness index (TWI)
The TWI shows the state of soil moisture, water depth, and topographic saturation zone (Moore et al., 1991).

$$TWI = In\left(\frac{AS}{\tan\beta}\right) \quad (2)$$

As depicts, the basin area and β is the land slope gradient (°).

2-5. Stream power index (SPI)
The stream power index represents the erosive power associated with the flow and the gravitational forces that move water downstream (Moore et al., 1991).

$$SPI = As \times \tan\sigma \quad (3)$$

As is the basin area and σ is the land slope gradient (°).

2-6. Normalized Difference Vegetation Index (NDVI)
VIS and NIR are visible and near-infrared spectral reflectance measurements, respectively (Massey et al., 1988).

$$NDVI = (NIR - (NIR + VIS) \quad (4)$$

$$S = 25.4\left(\frac{1000}{CN} - 10\right) \quad (5)$$

$$Q = \left(\frac{P-2S}{(P+8S)}\right) \quad (6)$$

P stands for precipitation (mm), S represents the number of primary abstractions (mm), and Q depicts the amount of runoff (mm).

2-7. Slope length factor (SLF)
The SLF describes the effects of topography and hydrology on soil erosion (Moore et al., 1991). SLF index is calculated using SAGA-GIS software by Equation (6).

$$SLF = (As/22.13)^{0.4} \times (\sin\beta/0.0896)^{1.3} \quad (7)$$

As is the upstream area (m^2), and β is the slope gradient in a given cell (°). The SLF values in the study area range from 0 to 266.

2-8. Topographic position index (TPI)
TPI represents the difference between a focal cell's height and neighboring cells' average height (Guisan et al., 1999). TPI is calculated using Equation (8).

$$TPI = Z_0 - \sum_{(1-n)} Z_n/n \quad (8)$$

Z_n is the height of the cells (m) in the window, Z_0 is the height of the evaluated cell (m), and n is the total number of neighboring cells used in the evaluation.

2-9. Terrain ruggedness index (TRI)
In the TRI, flat areas have a value of zero, while positive TRI values are found in mountainous areas with steep ridges (Dorn et al., 2014).

$$TRI = \sqrt{\sum_{P=1}^{8} ZMd} \quad (9)$$

P is the number of surrounding pixels, and ZMd is the average difference of eight pixels around each pixel.

2-10. Logistic regression model
Logistic regression is a multivariate statistical analysis considering several physical parameters that may affect the probability of flooding (Shirzadi et al., 2012). Logistic regression aims to determine an appropriate model to define the relationship between the dependent variable and the factors affecting flooding to generate coefficients for each variable (Lee et al., 2007). The logistic regression predicts the presence or absence of flooding as zero. In this research, to estimate flood sensitivity using the mentioned model for each of the network cells in the region, flood sensitivity has been evaluated using statistical modeling and the relationships of a set of environmental conditions (independent variables) and flood occurrence (dependent variable). The variables selected as flood risk predictors are topography, hydrology, lithology, and land use/cover. In implementing the logistic regression model, it is necessary to quantify all factors affecting the occurrence of floods. Land use, lithology, soil, and hydrologic units are qualitative and require meaningful codes. In this way, the qualitative layers (land use, lithology, and slope aspect) are arranged and coded in

descending order based on the effect of flooding in the basin. Then, in the SPSS environment, samples were taken from the available data, and a sample equal to 20 percent of the data was prepared. After this step, the logistic regression model is run. This study uses a step-by-step method to enter data into the logistic regression model. Dependent variables (y) are the occurrence and non-occurrence of floods. Independent variables (xi) are some environmental factors, including slope aspect, slope gradient, precipitation, land use/cover, lithology, elevation, and distance to river. 70% of floods in the region have been prepared using factors of the effective layer on flooding (independent variable). After entering the data into the model, the coefficients were extracted according to Table 2. In this study, the logistic regression model was chosen for its ability to analyze a two-state dependent variable (flood occurrence vs. non-occurrence) and for its accurate interpretation of the effects of independent factors such as rainfall, topography, and land use on the probability of a flood. This model, given its successful history in natural hazard zoning studies and its compatibility with spatial data in a GIS environment, allows the production of flood risk zoning maps with appropriate accuracy. In addition, the flexibility of logistic regression for handling incomplete data and its efficiency in limited-sample conditions make it a suitable option for this study.

2-11. Determining the CN

The CN is a variable and dimensionless parameter used in the SCS model to determine the initial loss parameter and the amplitude delay. After identifying the HSGs of the basin, the overlap of different layers, such as land use, is applied to determine the CN of the basin. After placing the basin soil HSGs to determine the CN of the basin using the digital elevation model of the land use map along with the basin soil map and creating its layer in the Arc GIS environment and overlapping these layers, the CN for soil and vegetation sets based on the average previous CN of mode II is estimated (Rustaei et al., 2017). The hypothetical average method was used to obtain the CN of the sub-basins. To this end, soil and land use maps overlapped, and homogeneous units were identified. Then the number of curves in each division was determined and multiplied by the covered area. When the sum of the multiplications was divided by the total area of the basin, the average CN was obtained.

Table 2. Coefficients of the logistic regression method.

	Independent variables	Coefficients
X0	Constant number	-2.36440721
X1	Slop	-0.00020103
X2	Density river	-0.000115544
X3	NDVI	-0.12234531
X4	Lithology	0.2236541
X5	Curvature	-0.4321598
X6	Elevation	0.229981
X7	Distance from river	-0.2581261
X8	TWI	-0.00036521
X9	SPI	0.3156987
X10	Rainfall	-0.3255143
X11	Land use	-0.000258741
X12	Aspect	-0.0011121
X13	Plan curvature	-0.0004281
X14	Profile curvature	-0.00261512
X15	Density river	-0.1235414
X16	Soil	-0.0012056
X17	SLF	-0.1361541
X18	TPI	-0.00002681
X19	TRI	-0.2654122

3. Results and Discussion

The slope is the determining factor in the speed of water movement and flow. Also, the water moves fast in lands with steep slopes. In the study area, the average slope area is 30 degrees. At a slope of 0-10 degrees, the water velocity increases, resulting in the peak hydrographic flow becoming faster. The state of the drainage network plays an important role in causing floods. Water flow in waterways is much faster than surface flow. Therefore, the higher the drainage density in a drainage basin, the higher the runoff accumulation rate and the steeper the ascent curve of the hydrograph will be. Examining the relationship between drainage density and a coefficient of 0.876 with the highest and a coefficient of 0.103 with the lowest value has the greatest effect on floods in the area, in which, some central, western, and southwestern parts of the basin have dense vegetation. As a result, water infiltration and runoff formation in this type of vegetation are reduced. Vegetation in the northern and eastern areas of the region is weak. As a result, the amount of water infiltration is low and increases the risk of flooding.

In some cases, lithology is the most important factor in flood control. Changes in lithological properties due to changes in rock resistance and permeability affect the intensity and distribution of floods (Fanni and Gheshmi, 2017). The siltstone unit is very sensitive to erosion and sedimentation, so erosional and grooved forms can be seen on them. On their surface, there are fine-grained pink soils with considerable thickness. The old alluvial defense unit has a high potential for erosion and sedimentation. Because their soil is very steep, the flood does not have much energy to reach them and lateral erosion is not seen in them. A young river's terrace unit has little erosion resistance due to the high density of waterways. The curvature of the slope shows the shape of the topography. Positive concavity indicates a surface where pixels are convex and negative concavity indicates a surface where pixels are concave. Zero (0) indicates that the surface is flat (Lee, 2004): flat lands have the greatest impact on floods. Topography plays an essential role in flooding. Flood flow is not the same on different surfaces (Green et al., 2014): most floods occur at an altitude of 1000-1500 meters. Flooding occurs near waterways, but it is less frequent at distances away from waterways (Wang et al., 2015). Most floods occur at a distance of 0 to 500 meters. The TWI shows the spatial distribution of humidity (Razavi Termeh and Malek, 2017). Slope classes 0-10 have the highest effects on floods. The SPI shows the erosive capacity of the waterway, which is directly related to the degree of slope and the basin's area. Slope classes 10-20 has the most effect in floods. Precipitation is an important factor in flooding. In the studied area, spring is the season of heavy rains and river flooding. In the studied area, more than 220 mm of precipitation has the greatest effect on the occurrence of floods. Human activities and land use/cover are effective factors in causing floods. The use of pasture has the greatest effect on the occurrence of floods in the study area. The topographic moisture index shows the amount of water accumulation in each pixel of the drainage basin.

The highest value of this STI index is 13, which is observed in all parts of the region. The sediment Transport Index (STI) indicates the strength of water flow in terms of erosivity, which affects hydrological conditions (Hong et al., 2018). The highest value of this index is observed in the northeastern regions of the area. SLF is a factor that describes the effects of topography and hydrology on soil erosion (Moore et al., 1991). In the study area, the northeastern areas of the region have the greatest impact on the occurrence of floods. The soil factor is an influential factor in controlling the rainfall-runoff mechanism (Xie et al., 2019). Aridisols are less prone to flooding due to higher permeability, and Entisols are more susceptible to flooding due to higher permeability. Profile curvature is the curvature along the line of maximum slope and is expressed as the change rate of slope aspects. The profile curvature indicates the intensity of water flow and transport and sedimentation processes. The flow speed increases in slope class 0-10, and the flood flows faster on this surface. The northern, eastern, and western slopes are prone to flooding due to heavy rain, long snow, and humidity. One of the most important factors in increasing flood damage is the irrational use of apparently favorable and potentially dangerous water resources exposed to

periodic floods. Areas adjacent to rivers are more affected by river floods, and the risk of flooding decreases by moving away from riverbeds. In most cases, the mentioned areas correspond to the flood plains of the region, which are always exposed to river floods (Figure 3).

3-1. Runoff

The SCS-CN equation has been used to estimate surface runoff for 5, 15, 25, and 50 years return periods. The CN parameter plays a vital role in estimating runoff and flood. To determine the CN, the area's soil, land use, vegetation density, and rainfall of the basin have been used (Figure 4). The amount of produced runoff has a direct relationship with floods, and regardless of other factors, the higher the amount of produced runoff in an area, the higher the probability of flood occurrences.

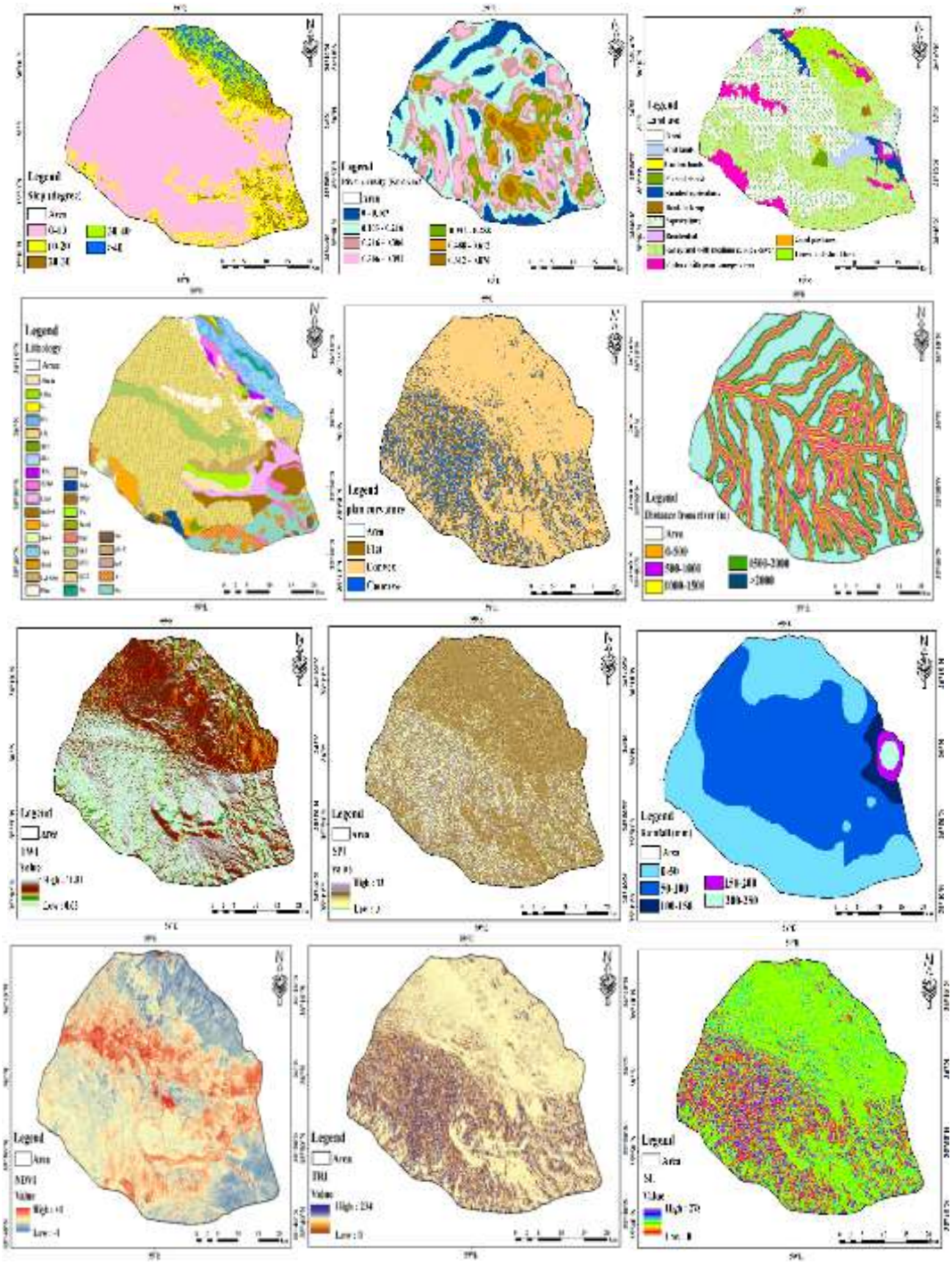

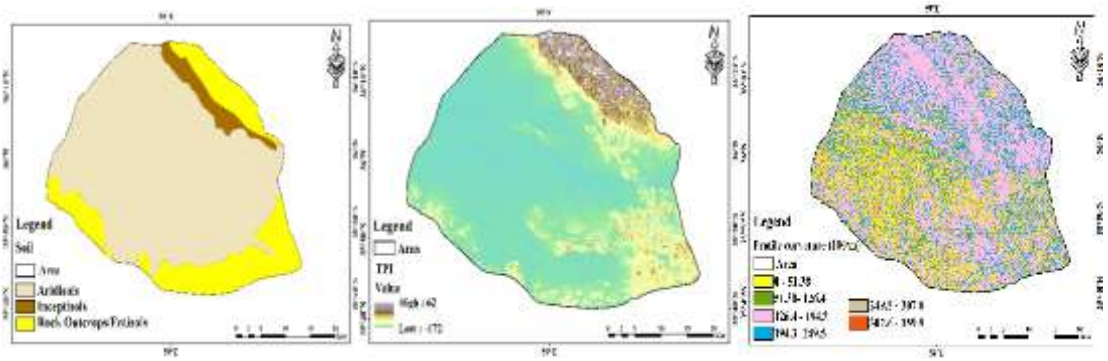

Figure 3. Factors affecting flood occurrence: Analysis of the impact of climatic, topographic, hydrological and human variables on increasing flood risk.

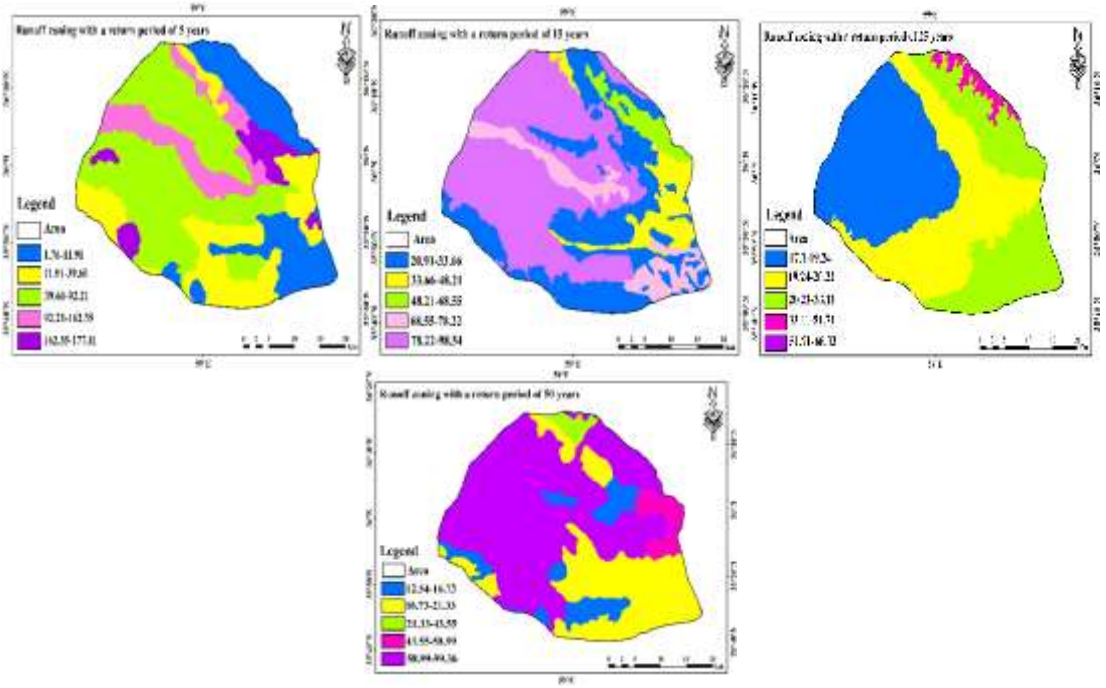

Figure 4. Maximum daily runoff with return periods of 5, 15, 25 and 50.

Figure 3 shows the maximum daily runoff discharge for 5, 15, 25, and 50-year return periods in the study area. The return period expresses the probability of a hydrological event (such as a flood) of a certain severity occurring within a given time interval. For example, a discharge with a 5-year return period represents the maximum discharge expected on average every 5 years, while a discharge with a 50-year return period represents rarer, more severe events. These analyses use historical hydrological data and statistical distribution curves (such as the Gumbel or Log-Pearson type III distribution) to estimate flood risk and design hydraulic structures. The results provide a scientific basis for flood risk zoning and water resource management in the region.

3-2. Hydrologic soil groups (HSGs)

Information on resource assessment, land capability and geological layers have been used to prepare the hydrological group map. This layer shows the rain penetrating the ground (Figure 5).

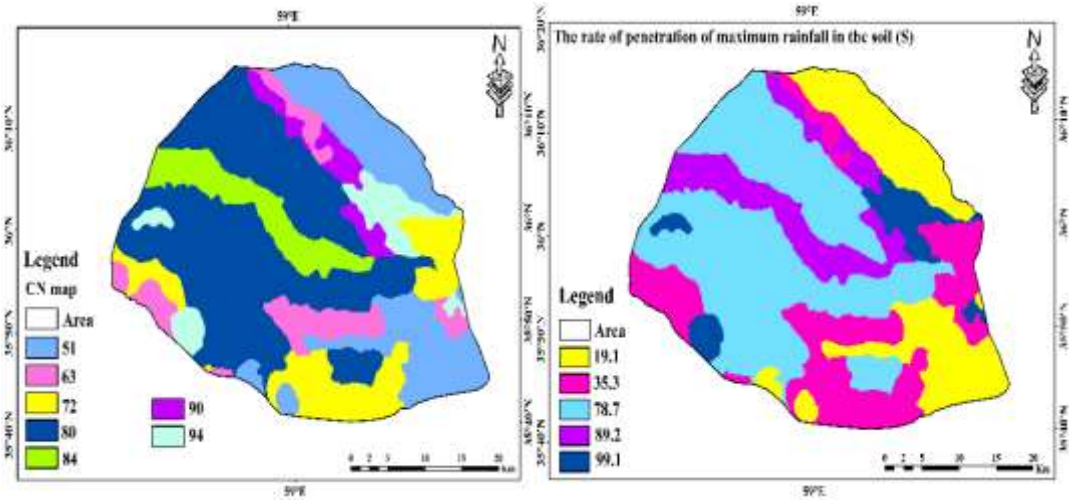

Figure 5. CN map and final infiltration map (S), (the unit of influence in the CN map is 0 or 1).

As Figure 5 illustrates, the effect of the CN coefficient in reducing the output flow rate is greater than the slope coefficient of the channel. Based on the sensitivity analysis of the parameters and the interpretation of the results presented in Figure 5, the effect of the CN coefficient (curve number) on the changes in the outflow is much greater than the effect of the channel slope coefficient. This is because CN, as an indicator of infiltration capacity and runoff production, has a nonlinear, direct impact on outflow volume. In contrast, the channel slope only changes flow velocity, with its effect on outflow volume being linear and limited. Therefore, small changes in CN can significantly alter outflow, whereas changes in channel slope have a negligible impact. Figure 5 also confirms this by showing changes in outflow across different scenarios. This reduction effect also works differently in sensitive hydrological units. The remarkable thing is the reverse effect of the slope of the waterways, which should be considered. In total, among the factors affecting the output of the basin in hydrological units, the most important and, at the same time, the simplest factor in terms of control and its effect on the output of the basin is the CN factor, which is mainly related to vegetation and the potential of runoff production in the area. The study is relatively large. The highest number of the runoff curve in high humidity conditions in the study area is 1.99, and the lowest value is 1.19. The high weighted average of the basin's CN indicates the basin's low permeability and the increased probability of flooding due to the presence of permeable soils. The results show that the highest CN is related to water lands, and the lowest CN is related to lands with good vegetation. In the map of hydrological groups, the highest percentage of the basin is related to groups with low permeability characteristics. In the land use map, land use with low soil permeability or non-permeable surface covers the largest area of the basin.

Then, the maps of precipitation zones with different 5, 15, 25, and 50 years return periods were prepared from the data related to maximum daily rainfall. After conducting relevant tests on data homogeneity and sufficiency, the amount of precipitation for the desired return periods was prepared using type 1 Gumbel[1] distribution. The potential use of the Gumbel distribution (Gumbel distribution describes the behavior of values of a maximum number of random samples) to represent the maximum relevant distribution is likely useful if the underlying sample data distribution is normal or exponential. This paper uses the Gumbel distribution to model the maximum value distribution. To model the minimum value, original negative values have been used. Nishabur rain gauge station has the highest precipitation amount, and Fadiyeh has the lowest. After applying weighting to the layers, based on their relationships and effects on flood stations, a standard function was employed for the weighted layers. Then the maximum precipitation was prepared for different return periods (Figure 6). As the investigations show, the flow rate has increased for a longer return period, and the

area is prone to flood occurrences. Of course, the difference in the expansion of the flood zone is primarily caused by topographical features. Wherever the width of the channel bed increases, the width of the flood surface also increases, and the runoff spreads over a wider area. The reason for the slight difference in flood levels in many places is the existence of steep topography. The regional results of flood zoning show that the highest percentage, i.e., 45 to 50 % of the basin area in all four return periods, is allocated to areas with moderate and high floods. These areas are mainly concentrated in the north, northeast, west, southeast, and center of the basin. Among them, the lowest percentage is related to the five years return period.

Examining the zoning maps shows that the flood-prone areas have the lowest slope. Also, the use of these lands is more of the poor pasture type, which creates suitable conditions for floods. The lowest flood potential in the region is directed to plains and low-lying areas, usually characterized by uses such as rainfed agriculture. The land slope gradient in these areas is at its lowest and below 10 degrees, which produces little runoff, which in turn has a significant effect on the flooding of a place. These changes have occurred mainly in the western parts of the basin, and other areas have remained almost constant. One of the basic and critical assumptions of logistic regression is that the error of each observation is independent of the error of other terms (no multiple correlations). The results of the logistic regression that shows the relationship between the occurrence of floods and the factors affecting the occurrence of floods are shown in Table 1. Data were analyzed by entering all independent and dependent variables, including 197 flood situations with codes 1, 30, and non-flood. Positions with a code of 0 were entered into the logistic regression statistical model (Table 3).

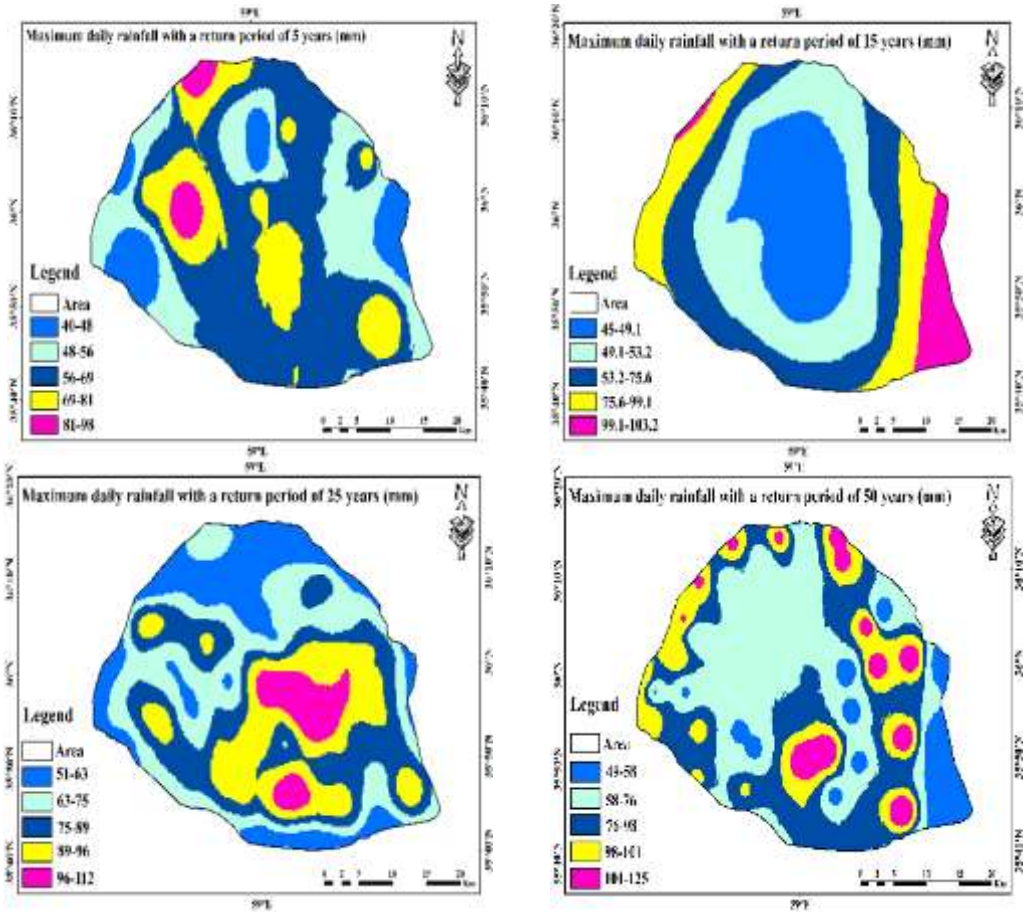

Figure 6. Rainfall map with return period of 5, 15, 25 and 50 years.

Table 3. Spatial factor coefficients in the Logistic Regression Method.

%95 C.I. For e^B (confidence interval)		e^B (Odds ratios associated with a change in predictor scores)	sig (Significance level)	df (Equivalent to the difference in the number of coefficients)	Wald (Parametric test)	S.E (Variable coefficient)	B (The width of the regression origin)	Factor	Method
upper	Lower								
1.076	0.626	12.111	0.001	1	10.213	0.9	2.31	Slope	Enter
0.961	0.999	18.323	0.05	1	11.011	0.654	3.41	Lithology	
2.066	0. 728	6.171	0.113	1	0.421	0.001	1.71	Density river	
1.071	0.355	0.153	0.211	1	0.312	0.067	-0.001	Land curvature	
1.023	0.489	6.322	0.101	1	0.077	1.003	1.22	Elevation	
0.961	0.978	28.221	0.05	1	13.251	0.989	4.12	Distance from rivers	
1.099	0.728	4.525	0.271	1	0.621	1.002	1.66	TWI	
1.089	0.711	3.212	0.266	1	0.789	0.001	1.52	SPI	
1.044	0.714	12.101	0.454	1	0.011	0.7	0.1	Land use	
0.978	0.933	21.211	0.05	1	8.516	0.921	3.91	NDVI	
1.036	0.868	11.179	0.001	1	6.371	0.02	2.31	Rainfall	
1.714	0.891	12.254	0.001	1	4.459	0.823	2.83	Runoff	
1.623	0.688	11.763	0.373	1	0.853	1.006	1.56	Hydrologic soil groups	
1.412	0.654	11.23	0.154	1	1.156	0.123	2.11	Aspect	
1.265	0.423	13.11	0.236	1	1.194	0.213	1.36	plan curvature	
1.522	0.398	17.33	0.458	1	1.354	0.154	0.002	profile curvature	
1.754	0.796	22.113	0.622	1	0.613	0.312	2.21	Soil	
1.623	0.811	14.31	0.005	1	0.456	0.112	1.91	SLF	
1.722	0.901	14.56	0.008	1	0.513	0.312	1.63	TPI	
1.098	0.725	16.64	0.698	1	0.752	0.352	0.04	TRI	
1.721	0.841	2.413	0.731	1	0.058	6.103	1.085	Fixed	

According to the coefficients of the independent variables, it can be concluded that lithology, distance to waterway, and NDVI are effective factors in the occurrence of floods in the study basin. For fitting the regression coefficients, the existing flood

layer Y is the response variable, and the layer of variables affecting the occurrence of floods is variable X. In addition to the 197 flooded points identified in the study area, another 110 locations were randomly selected throughout the basin. After covering the layers, they were divided into classes, such as the presence of flooded points, code 1, etc. Regarding non-flooded points, influential factors such as non-flooded points were coded as 1 and other types as 0. After entering the data into the model, statistical analysis was performed, and finally, the coefficients of the classes of independent and dependent variables were assigned. After applying the coefficients obtained from the model, the independent variables of the linear parameter Z were prepared. Negative weights for logistic regression coefficients indicate that flood occurrence is negatively correlated with independent variables. For the earth curvature coefficient, the weighted values are negative. The distance to waterway, with a value of 4.12, has the greatest weight in the occurrence of floods. The significance level of 0.05 indicates a statistically significant effect of the influencing factor on floods. The most influential factors in terms of geological importance are the distance to waterway/river and NDVI. The difference in the negative two log-likelihood (-2LL) is considered an effective indicator of model improvement in the null model (Table 4). The minimum value of -2LL provides the best GoF model for the data and describes the reduction values until the final iteration step. Cox/snels and Nagelkerke's R-squared are employed to measure the model. The higher the R-squared, the better the model will be (Althuwaynee et al., 2014). Equation (9) prepared the flood sensitivity map (Figure 6).

Table 4. Table of Logistic Regression Method.

Metod	Step	-2log likelihood	Cox/snells R-square	Negelkerkes R-square
Enter	1	40.59 4a	0.701	0.951

$$p = (\text{flood susceptibility}) = \frac{ez}{1+ez} \quad (9)$$

Z = 2.31 × slope– 3.41 × Lithology– 1.71 ×Density river–0.001 × Curvature– 1.22 × Elevation– 4.12 × Distance from river– 1.66 × TWI – 1.52 × SPI– 2.87 × Rainfall – 0.1 × Land use – 3.91 × NDVI – Rainfall × 2.31 – Hydrologic soil groups × 1.56 – Runoff ×Aspect– 2.11 ×plan curvature – 1.36 ×profile curvature – 0.002 ×Soil – 2.21 ×SLF – 1.91 × TPI – 1.63 × TRI – 0.04

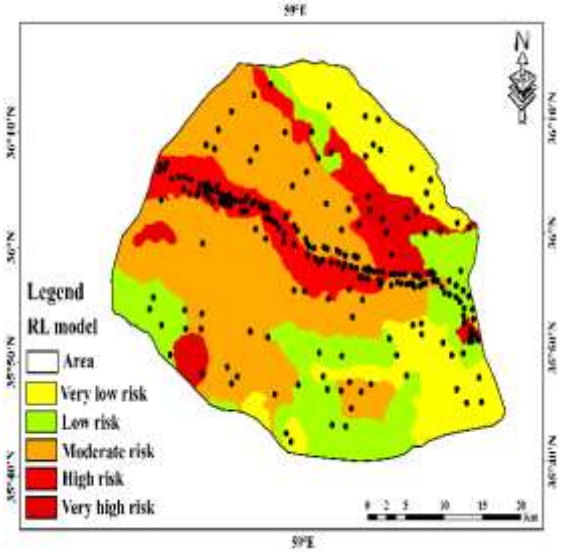

Figure 6. Flood susceptibility zoning map with Logistic Regression model.

3-3. Validation of the flood susceptibility map

Validation of prepared maps is essential in determining flood-prone areas and their quality (Pourghasmi et al., 2013). The ROC curve is a visual representation of the balance between negative and positive error rates for any possible value of cutoff points or AUC. The area under the ROC curve represents the prediction value of the system by describing its ability to correctly estimate flood occurrence and non-occurrence. Floods that happened (flood occurrence) and events that did not happen (no flood occurrence) (Lee et al., 2017). In ROC curves, the specificity or false positive rate is shown on the X axis, and the sensitivity or true positive rate is shown on the Y axis. The TPR (sensitivity) is plotted against the FPR (1-specificity) for each possible cutoff value of the accuracy assessment. The TPR (sensitivity) and the FPR (1-specificity) were calculated via Equations (10), (11), and (12) (Chen et al., 2018).

$$\text{Sensitivity} = \frac{\text{TP}}{(\text{TP}+\text{FN})} \quad (10)$$

$$1 - \text{Specificity} = 1 - \left[\frac{\text{TN}}{\text{FP}+\text{TN}}\right] \quad (11)$$

$$\text{AUC} = \frac{(\sum \text{TP}+\sum \text{TN})}{\text{P}+\text{N}} \quad (12)$$

TP stands for True Positive (True Pixel), classified as a correct prediction (flood occurrence). TN stands for True Negative. Pixels that are correctly classified as False Positive (FP) predictions (flood non-occurrence) are FPs, and pixels that are incorrectly classified as flood occurrence are False Negatives (FNs), and pixels are incorrectly classified as flood non-occurrence. *P* is the total number of flood occurrences (correct prediction), and *N* is the number of independent realizations of a model probability distribution. Data from flooded areas and several other random pixels from non-flooded areas were prepared to use the ROC curve in this study. Due to the existence of 1174 pixels for flood-prone areas in the map, at the end, 1174x2 matrices were created for each zoning model to check the estimates of flood occurrence or non-occurrence in risk categories. Therefore, flood risk maps were evaluated using the ROC curve and considering the area under the curve. The results showed that the prediction rate for the logistic regression model is AUC 0.815 and for the CN model AUC 0.921, indicating the high accuracy of the models (Figure 7).

Then, the performance of the models was evaluated using appropriate GoF criteria, such as root mean square error (RMSE) and mean absolute error (MAE). The above statistical criteria alone are insufficient to evaluate the models because RMSE and MAE are based on error evaluation (Panahi et al., 2021). The results obtained from the two models used are shown in Table 5, illustrating that the SCS-CN model performs best for modeling flood-prone areas following the observational events (the highest AUC value and the lowest StD, MSE, and RMSE values). The SCS-CN model performance based on the AUC is an average 5% performance improvement.

3-4. The SCS-CN model

The value of each score has been considered to weight the layers according to the AHP method and according to the opinions. Finally, the layers were combined, and a flood-prone zonation map was obtained (Equation 13). Table 4 shows the class and weight assigned to each factor.

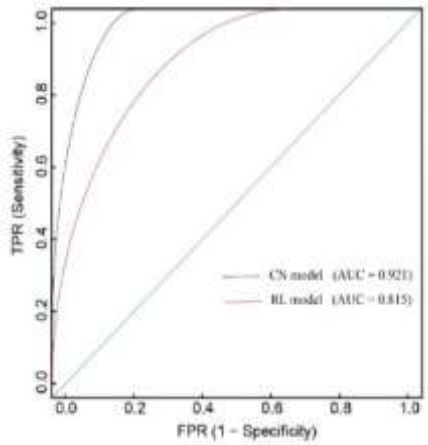

Figure 7. ROC curve of Logistic Regression model and CN model.

Table 5. Scores of factors affecting the occurrence of floods.

The final weight of the layers	Criterion
0.033	Runoff
0.048	Hydrologic soil groups
0.151	Slope
0.054	Lithology
0.181	Density river
0.023	Land curvature
0.041	Elevation
0.058	Distance from river
0.69	TWI
0.078	SPI
0.199	Rainfall
0.191	Land use
0.083	NDVI
0.071	Aspect
0.081	Plan curvature
0.041	Profile curvature
0.099	Soil
0.015	SLF
0.085	TPI
0.089	TRI

$$\text{Flooding} = 0.151 \times \text{Slope} + 0.054 \times \text{Lithology} + 0.181 \times \text{Density river} + 0.001 \times \text{Curvature} + 0.044 \times \text{Elevation} + 0.058 \times \text{Distance from river} + 0.069 \times \text{TWI} + 0.078 \times \text{SPI} + 0.199 \times \text{Rainfall} + 0.191 \times \text{Land use} + 0.083 \times \text{NDVI} + 0.048 \times \text{Hydrologic soil groups} + 0.033 \times \text{Runoff} + 0.083 \times \text{NDVI} \times \text{Aspect} + 0.071 \times \text{plan curvature} + 0.081 \times \text{profile curvature} + 0.041 \times \text{Soil} + 0.099 \times \text{SLF} + 0.015 \times \text{TPI} + 0.085 \times \text{TRI} + 0.089 \quad (13)$$

By performing Equation (13) on the layers, the flood map with the 5, 15, 25, and 50 years return periods of the basin was obtained (Figure 8). According to the map, the flood-prone area is located in the northern and western parts of the highlands. Examining the layers used in flood zoning shows these areas have a slope of less than 30°. Also, these areas include poor rainfed pastures. Flooding conditions are less in the eastern areas due to lower slope, dense vegetation and drainage density. The slope of the land in these areas is 5°, which causes less runoff. The land use change in the region is diverse in different places. The conversion of forest land to agriculture, pasture land to agriculture, and agricultural land to abandoned land are among these changes. In the northern and northeastern parts of the basin, severe land damage and its change to irrigated lands can be observed. The conversion of agricultural land to pasture is maintained in the southern and southwestern parts of the basin. As a result, it affects the value of the curve of the basin, especially in the mentioned areas, and causes an increase in the number of curves. The classes that have the potential of runoff are water lands that are generally located in the northeast and southeast of the region.

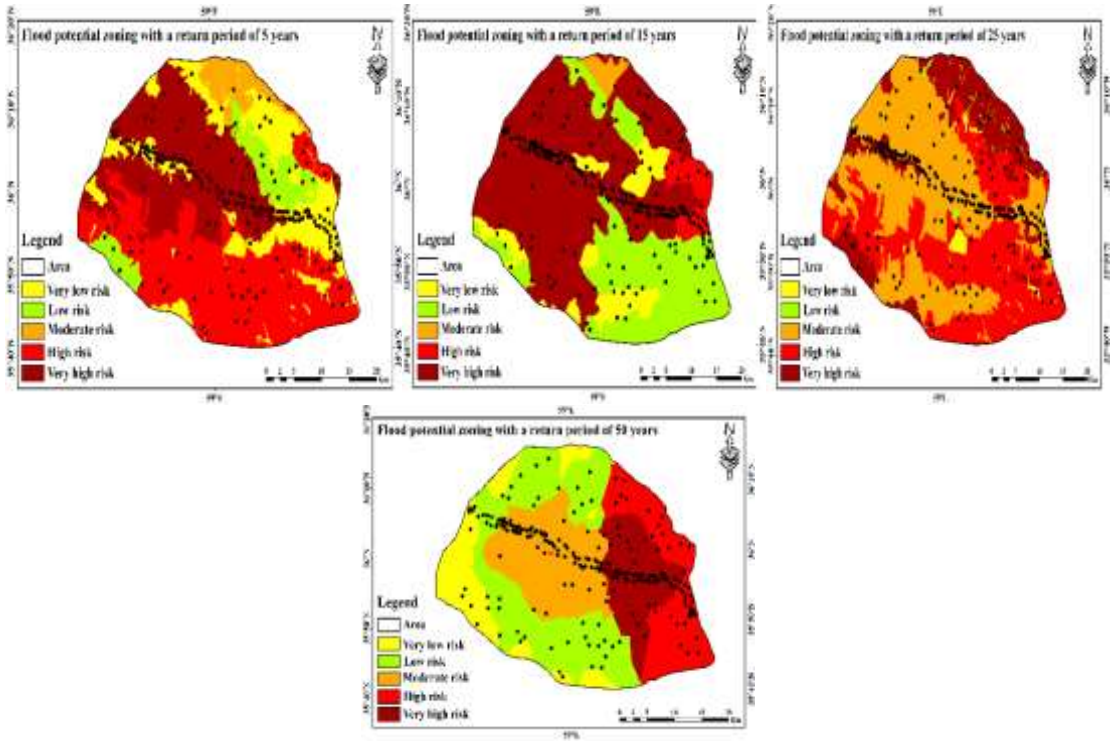

Figure 8. Flood potential zoning with return period of 5, 15, 25 and 50 years.

4. Conclusion

The northern and western parts of the basin are in high-risk and very high-risk classes. Its main reasons are low altitude, low slope gradient, poor vegetation, high drainage density, and convex surfaces. Runoff is lower in areas with dense vegetation, resulting in reduced floods. Therefore, in areas with low or moderate flooding, the levels of CN and Q decrease, and the *S* factor increases. The results show that the SCS-CN model has high speed and accuracy in preparing the flood zoning map, and the predictions are very close to the existing reality. Examining the parameters affecting the occurrence of floods shows that various environmental and human factors cause an increase in floods in the basin. Among the human factors, the change in land use, the creation of inappropriate constructions in the vicinity of waterways, the destruction of the slope due to plowing and turning it into agricultural land, and the destruction of vegetation due to the excessive grazing of livestock can be mentioned. Natural factors include low slopes, torrential rains, impermeable sediments, and soft and erodible formations. Considering the physical characteristics of the basin, including the area, low permeability, and low concentration time, especially in recent years, the height of the basin's runoff has increased, and destructive floods have caused problems in Kalateh-ye Qanbar Drainage Basin. Using flood estimation methods, flood discharge with longer than 5-50 years return periods produces more flood volume. The results of this study showed that the combined AHP method for layer weighting and the SCS-CN model for estimating hydrological response can produce flood risk zoning maps for 5, 15, 25, and 50-year return periods with acceptable accuracy. The AUC value of 0.81 indicates the model's appropriate accuracy in identifying high-risk areas, consistent with the range reported in studies by Kader et al. (2024). Studies that have used only MCDM methods such as AHP have also been able to identify high-risk areas with reasonable accuracy; the overall spatial results (risk concentration in the northern and western parts of the basin due to low slope, high drainage density, and poor vegetation cover) are consistent with the patterns reported in regional studies, and with the results of the study by Seydi et al. (2023). Recent studies have also proposed and implemented statistical validation methods, such as the ROC/AUC curve, to assess the reliability of zoning maps. Therefore, the current research approach to validation using logistic regression and ROC is consistent with the study by Al-Areeq et al. (2022). However,

the study by Abu El-Magd et al. (2022) shows that machine learning and hybrid methods can increase accuracy more than traditional methods; some studies have reported that machine learning models or hybrid frameworks can achieve higher AUC. On the other hand, the finding that dense vegetation reduces runoff and risk is confirmed by Hong (2025), which emphasizes the need for nature-based methods for flood mitigation. According to the flood risk zoning map, appropriate management measures can be taken to reduce flood damage with the two mentioned models. Among them, we can mention the construction of dams to reduce water flow, store, and accumulate water by observing the following points. The principles of river engineering according to the conditions of the study drainage basin and the implementation of structural plans for flood control, modification, and protection of the river course to stabilize the bed and control erosion, and improve and increase the capacity of drainage basins.

Declarations

Funding: The authors did not receive support from any organization for the submitted work.

Declarations of interests: The authors declare that they have no competing interests.

Data Availability Statement: All data generated or analyzed during this study are included in this published article.

References

Abedini, M., & Lotfi, Kh. (2019). Estimating the height of runoff to analyze flood potential using the curve number method in the Shahrood catchment area of Ardabil, *Quarterly of Geographic Space* (19) 68. 163-181.

Abu El-Magd, S. A., Maged, A., & Farhat, H. I. (2022). Hybrid-based Bayesian algorithm and hydrologic indices for flash flood vulnerability assessment in coastal regions: machine learning, risk prediction, and environmental impact .*Environmental Science and Pollution Research*, 29 (38), 57345–57356. https://doi.org/10.1007/s11356-022-19903-2.

Aditian, A., Kubotab, T., & Shinoharab, Y. (2018). Comparison of GIS-based landslide susceptibility models using frequency ratio, logistic regression, and artificial neural network in a tertiary region of Ambon, Indonesia. *Geomorphology*, 318, 101–111.

Ahmadlou, M., Karimi, M., Alizadeh, S., Shirzadi, A., Parvinnejhad, D., Shahabi, H., & Panahi, M. (2019). Flood susceptibility assessment using integration of Adaptive Network-Based Fuzzy Inference System (ANFIS) and Biogeography-Based Optimization (BBO) and BAT Algorithms (BA). *GeocartoInternational*, 34 (11),1252-1272.

Al-Areeq, A. M., Abba, S. I., Yassin, M. A., Benaafi, M., Ghaleb, M., & Aljundi, I. H. (2022). Computational Machine Learning Approach for Flood Susceptibility Assessment Integrated with Remote Sensing and GIS Techniques from Jeddah, Saudi Arabia . *Remote Sensing*, 14 (21), 5515. https://doi.org/10.3390/rs14215515.

Althuwaynee, O. F., Pradhan, B., Park, H. J., Lee, J. H. (2014). A novel ensemble bivariate statistical evidential belief function with knowledge-based analytical hierarchy process and multivariate statistical logistic regression for landslide susceptibility mapping. *Catena*, 114, 21–36.

Bates, P. D., Horritt, M. S., & Fewtrell, T. J. (2010). A simple inertial formulation of the shallow water equations for efficient two dimensional flood inundation modelling. *J. Hydrol*, 387, 33–45. doi: 10.1016/j.jhydrol.2010.03.027.

Bui, D. T., Tsangaratos, P., Ngo, P. T. T., Pham, T. D., & Pham, B. T. (2019). Flash flood susceptibility modeling using an optimized fuzzy rule based feature selection technique and tree based ensemble methods. *Sci. Total Environ*, 668, 1038–1054.

Cai, X., & Xu, D. (2022) Simulation and Optimization Strategy of Storm Flood Safety Pattern Based on SCS-CN Model. *Int. J. Environ. Res. Public Health*, 19, 698. https://doi.org/10.3390/ijerph19020698.

Chen, W., Peng, J., Hong, H., Shahabi, H., Pradhan, B., Liu, J., Zhu, A., Pei, X., & Duan, Z. (2018). Landslide susceptibility modelling using GIS-based machine

learning techniques for Chongren County, Jiangxi Province, China. *Sci. Total Environ*, 626, 1121–1135. https://doi.org/ 10.1016/j.scitotenv.2018.01.124.

Costache, R., & Bui D. T. (2020). Identification of areas prone to flash-flood phenomena using multiple-criteria decision-making, bivariate statistics, machine learning and their ensembles. *Sci. Total Environ*, 136492.

Crawford, N. H. (1966). Digital Simulation in Hydrology: Stanford Watershed Model IV; Stanford University Technical Reports; Department of Civil Engineering, Stanford University: Stanford, CA, USA: 39.

Darabi, H., Torabi Haghighi, A., Rahmati, O., Jalali Shahrood, A., Rouzbeh, S., Pradhan, B., & Tien Bui, D. (2021). A hybridized model based on neural network and swarm intelligence-grey wolf algorithm for spatial prediction of urban flood-inundation. *Journal of Hydrology*, 603, 126854. 1-11.

Dodangeh, E., Choubin, B., Eigdir, A. N., Nabipour, N., Panahi, M., Shamshirband, S., & Mosavi, A. (2020) .Integrated machine learning methods with resampling algorithms for flood susceptibility prediction. *Sci. Total Environ*, 705, 135983.

Dorn, J., Bourgeois, J., Bats, M., Zwertvaegher, A., Gelorini, V., De Smedt, P., Chu, W., Antrop, M., De Maeyer, P., Finke, P., Van Meirvenne, M., Verniers, J., & Cromb´e, P. (2014) Application of the topographic position index to heterogeneous landscapes. *Geomorphology*, 186, 39.

Dottori, F., Salamon, P., Bianchi, A., Alfieri, L., Hirpa, F. A., & Feyen, L. (2016). Development and evaluation of a framework for global flood hazard mapping. *Adv. Water Resour*. 94, 87–102. doi: 10.1016/j.advwatres.2016.05.002.

El-Rawy, M., Elsadek, W. M., & De Smedt, F. (2022). Flash Flood Susceptibility Mapping in Sinai, Egypt Using Hydromorphic Data, Principal Component Analysis and Logistic Regression. *Wate*r, 14, 2434. https://doi.org/10.3390/ w14152434.

Fang, Sh., Ji, Y., & Zhang, M. (2022). Numerical Modeling the Flood and Pollutant Transport Processes in Residential Areas with Different Land Use Types. *Hindawi Advances in Meteorology*, 16, Doi.org/10.1155/2022/9320089.

Fanni, Z, & Gheshmi, S. (2017). Spatial zoning and analysis of the four environmental hazards of landslides, floods, earthquakes and subsidence (Case study: 22 districts of Tehran). *Journal of Geographical Data (SEPEHR)*, 27 (4), 76-89.

Garrote, J. (2022). Global DEMs and Flood Modelling - A Comparison Analysis for the January 2015 Flooding Event in Mocuba City (Mozambique). *Water*, 14 - (176), Doi.org/10.3390/w14020176.

Gholami, H., Mohammadifar, A., Golzari, Sh., Torkamandi, R., Moayedi, E., Zare Reshkooeiyeh, M., Song, Y., & Zeeden, Ch (2025). Mapping flood risk using a workflow including deep learning and MCDM– Application to southern Iran. *Urban Climate*, 59, 102272, https://doi.org/10.1016/j.uclim.2024.102272

Green, C, Diepernk, G., Hegger, D., Pettersson, M., Priest, S., & Tapsell, S. (2014) Flood risk management in Europe: the flood problem and interventions. *Star flood*, 1- 250.

Guisan, A., Weiss, S. B., & Weiss, A. D. (1999). GLM versus CCA spatial modeling of plant species distribution. *Plant Ecol*, https://doi.org/10.1023/A:1009841519580

Hawkins, R. H. (1980). "Sit selection and curve numders", Proceeding of symposium on watershed management, ASAE, Littleton, co.USA.

He, X., Chen, Ch., & Liu, Y. (2019). Mountain flooding analysis based on SCS-CN model -- A case study in Mingxi, China, IOP Conf. Series, *Materials Science and Engineering*, 780, 072048. doi:10.1088/1757-899X/780/7/072048.

Hitouri, S., Mohajane, M., Lahsaini, M., Ali, S. A., Setargie, T. A., Tripathi, G., D'Antonio, P., Singh, S.K., & Varasano, A. (2024). Flood Susceptibility Mapping Using SAR Data and Machine Learning Algorithms in a Small Watershed in Northwestern Morocco. *Remote Sens*, 16, 858. https://doi.org/10.3390/rs16050858.

Hong, H., Tsangaratos, P., Ilia, I., Liu, J., Zhu, A. X., & Chen, W. (2018).

Application of fuzzy weight of evidence and data mining techniques in construction of16 D. TADESSE ET AL.flood susceptibility map of Poyang County, China.Science of the Total Environment, 625, 575–588. https://doi.org/10.1016/j.scitotenv.2017.12.256.

Hong, J. (2025). Improving flood hazard susceptibility assessment by integrating hydrodynamic modeling with remote sensing and ensemble machine learning . *Natural Hazards*.https://doi.org/10.1007/s11069-025-07109-2.

Hosein, Y. (2022). Evaluation of WMS model in basins without statistical data in southwestern Iran using Dicken's experimental method (case study: Kuhgel Basin of Khuzestan Province). *Applied Water Science*, 12, 162 https://doi.org/10.1007/s13201-022-01685-5.

Islam, T., Zeleke, E. B., Afroz, M., & Melesse, A. M. A. (2025). Systematic Review of Urban Flood Susceptibility Mapping: Remote Sensing, Machine Learning, and Other Modeling Approaches. *Remote Sens*, 17, 524.https://doi.org/10.3390/rs17030524.

Jehanzaib, M., Ajmal, M., Achite, M., & Kim, T. W. (2022). Comprehensive Review: Advancements in Rainfall-Runoff Modelling for Flood Mitigation. *Climate*, 10, 147. https://doi.org/10.3390/cli10100147

Kader, Z., Islam, M. R., Aziz, M. T., Islam, M. R., & Miah, M. (2024). GIS and AHP-based flood susceptibility mapping: a case study of Bangladesh . *Sustainable Water Resources Management*, 10, 170. https://doi.org/10.1007/s40899-024-01150-y.

Khosravi, K., Melesse, A. M., Shahabi, H., Shirzadi, A., Chapi, K., & Hong, H. (2019). Flood susceptibility mapping at ningdu catchment, China using bivariate and data mining techniques". *Extreme Hydrology and Climate Variability*, 419–434, Amsterdam e Netherlands.

Khosravi, K., Shahabi, H., Pham, B. T., Adamowski, J., Shirzadi, A., Pradhan, B., & Prakash, I. (2019). A comparative assessment of flood susceptibility modeling using multi-criteria decision-making analysis and machine learning methods. *Journal ofHydrology*, 573, 311-323.

Kia, M. B., Pirasteh, S., Pradhan, B., Mahmud, A. R.,Sulaiman, W. N. A., & Moradi, A. (2012). An artificial neural network model for flood simulation using GIS:Johor River Basin, Malaysia. *Environmental Earth Sciences*, 67, 251–264. https://doi.org/10.1007/s12665-011-1504-z.

Lee, S. (2004). Application of likelihood ratio andlogistic regression models to landslide susceptibilitymapping using GIS. *Environmental Management*, 34 (2), 223-232.

Lee, S., & Pradhan, B. (2007). Landslide hazard mapping at Selangor, Malaysia using frequency ratio and logistic Regression Models. *Landslide*s, 4 (33), 33-41.

Lee, S., Lee, M. J., & Jung, H. S. (2018). Spatial assessment of urban flood susceptibility using data mining and geographic information system (GIS) tools. *Sustainability*, 10 (3), 648.

Linusa, J., Tanjayaa, V., & Kurniawan, A. (2024). Performance Comparison of Machine Learning Methods for Flood Prediction, 9th International Conference on Computer Science and Computational Intelligence 2024 (ICCSCI 2024), Procedia Computer Science 245. 1040–1046.

Lyu, H., Zhou, W., Shen, S., & Zhou, N. (2020). Inundation risk assessment of metro system using AHP and TFN-AHP in Shenzhen. *Sustainable Cities and Society*, 56, https://doi.org/10.1016/j.scs.2020.102103.

Mahdavi, M. (2023). Applied hydrology, 1st edition. Tehran: Tehran University Press.

Massey, A., Douglas, S., & Denton, A. (1988). The Dimensions of Residential". *Social Forces*, 67 (2), 281–315.

Mekanik, F., Imteaz, M., Gato-Trinidad, S., & Elmahdi, A. (2013). Multiple regression and Artificial Neural Network for long-term rainfall forecasting using large scale climate modes. *J. Hydrol*, 503, 11–21.

Mohammadi, H., & Panahi, A. (2006). Estimation of runoff using SCS and GIS in Ghale Chay watershed (East azarbaijan province), *Iranian journal of*

geographical association. New Period of 10 and 11 Autumn and Winter, 109-123.

Moore, I. D., Grayson, R. B., & Ladson, A. R. (1991). Digital terrain modelling: A review of hydrological, geomorphological. and biological applications. *Hydrol. Process*, doi: 10.1002/hyp.3360050103.

Mosavi, A., Rabczuk, T., & Varkonyi-Koczy, A. R. (2017). Reviewing the novel machine learning tools for materials design. *Int. Conf. Glob. Res. Educat*, 50–58.

Nachappa, T. G., Piralilou, S. T., Gholamnia, K., Ghorbanzadeh, O., Rahmati, O., & Blaschke, T. (2020). Flood susceptibility mappingwith machine learning, multi-criteria decision analysis and ensemble using Dempster Shafer Theory. *Journal of Hydrology*, 590, 125275.

Nguyen, V. N., Bui, D. T., Ngo, P. T., Nguyen, Q. P., Nguyen, V. C., Long, N. Q., & Revhaug, I. (2017). An integration of least squares support vector machines and firefly optimization algorithm for flood susceptible modeling using GIS. *Presented at the International Conference on GeoSpatial Technologies and Earth Resources*, Springer: 52–64.

Obada, E., Biaoa, E. I., Zohouc, P. J., Yaroud, H., Hounnondahoa, F. Z., & Alamoua, E. A. (2025). Using machine learning and satellite data to improve flood forecasting: the case of the Ouémé basin at the Bétérou outlet. *Hydrology Research*, 56, 2, 153, doi: 10.2166/nh.2025.133.

Panahi, M., Dodangeh, E., Rezaie, F., Khosravi, K., Van Le, H., Lee, M. J., & Thai Pham, B. (2021). Flood spatial prediction modeling using a hybrid of metaoptimization and support vector regression modeling. *Catena*, 199,105114.

Pavesi, L., Volpi, E., & Fiori, A. (2024). Flood risk assessment through large-scale modeling under uncertainty, *Nat. Hazards Earth Syst. Sci*, 24, 4507–4522, 2024, https://doi.org/10.5194/nhess-24-4507-2024.

Polykretis, C., & Chalkias, C. (2018). Comparison and evaluation of landslide susceptibility maps obtained from weight of evidence, logistic regression, and artificial neural network models. *Nat Hazards*, 93, 249–274. https://doi.org/10.1007/s11069-018-3299-7

Pradhan, B. (2010). Flood susceptible mapping and risk area delineation using logistic regression, GIS and remote sensing. *J Spat Hydrol*, 9(2),1–18.

Prein, A. F., Rasmussen, R. M., Ikeda, K., Liu, C., Clark, M. P., & Holland, G. J. (2017). The future intensification of hourly precipitationextremes. *Nature Climate Change*, 7(1), 48–52.

Razavi Termeh, S.V., & Malek, M. R. (2017). Preparation of flood susceptibility mapping using an ensemble of frequency ratio and adaptive neuro-fuzzy inference system models (Case study: Jahrom Township). *Journal of Geomatics Science and Technology*, 8(3), 1-15.

Rozalis, S., Morin, E., Yair, Y., & Price, C. (2010). Flash floodprediction using an uncalibrated hydrological model andradar rainfall data in a Mediterranean watershed underGEOLOGY, ECOLOGY, AND LANDSCAPES 17changing hydrological conditions. *Journal of Hydrology*, 394 (1–2), 245–255. https://doi.org/10.1016/j.jhydrol.2010.03.021.

Rudari, R., Silvestro, F., Campo, L., Rebora, N., Boni, G., & Herold, C. (2015). Improvement of the Global Flood Model for the GAR 2015. *Geneva*, United Nations.

Sahana, M., Rehman, S., Sajjad, H., & Hong, H. (2020). Exploring effectiveness of frequency ratio and support vector machine models in storm surge flood susceptibility assessment: A study of Sundarban Biosphere Reserve, India. *Catena*, 189, 104450.

Samanta, S., Pal, D. K., & Palsamanta, B. (2018). Flood susceptibility analysis through remote sensing, GIS and frequency ratio model. *Applied Water Science*, 8, 66.

Sampson, C. C., Smith, A. M., Bates, P. B., Neal, J. C., Alfieri, L., & Freer, J. E. (2015). A high-resolution global flood hazard model. *Water Resour. Res*, 51, 7358–7381. doi: 10.1002/2015WR016954.

Santos, P. P., Reis, E., Pereira, S., & Santos, M. (2019). A flood susceptibility model at the national scale based on multicriteria analysis. *Science of The Total Environment*, 667, 325-337,

https://doi.org/10.1016/j.scitotenv.2019.02.328.

Schumann, G. J. P., Stampoulis, D., Smith, A. M., Sampson, C. C., Andreadis, K. M., & Neal, J. C (2016). Rethinking flood hazard at the global scale. *Geophys. Res. Lett*, 43, 249–256, doi: 10.1002/2016GL070260.

Seydi, S. T., Kanani-Sadat, Y., Hasanlou, M., Sahraei, R., Chanussot, J., & Amani, M. (2023). Comparison of Machine Learning Algorithms for Flood Susceptibility Mapping. *Remote Sensing*, 15 (1), 192. https://doi.org/10.3390/rs15010192.

Shahabi, H., Shirzadi, A., Ghaderi, K., Omidvar, E., Al-Ansari, N., Clague, J. J., Geertsema, M., Khosravi K., Amini, A., Bahrami, S., & Rahmati, O. (2020). Flood detection and susceptibility mapping using sentinel-1 remote sensing data and a machine learning approach: Hybrid intelligence of bagging ensemble based on k-nearest neighbor classifier. *Remote Sens*, 12 (2), 266.

Shatnawi, A., & Ibrahim, M. (2022). Derivation of flood hydrographs using SCS synthetic unit hydrograph technique for Housha catchment area. *Water Supply*, 22, 4888 doi: 10.2166/ws.2022.169.

Shirzadi, A., Saro, L., Joo, O. H., & Chapi, k. (2012). A gis based logistic regression model in roak fall susepitbility mapping along a mountainous road : salavat abad case study, Kurdistan , iran. *Natural hazard*, 64, 1639- 1656.

Soma, A. S., Kubota, T., & Mizuno, H. (2019). Optimization of causative factors using logistic regression and artificial neural network models for landslide susceptibility assessment in Ujung Loe Watershed, South Sulawesi Indonesia. *J Mt Sci*, 16, 144–162. https://doi.org/10.1007/s11629-018-4884-7.

Sulaiman, J., & Wahab, S. H. (2017). Heavy rainfall forecasting model using artificial neural network for flood prone area. *Lecture Notes Electr Eng*, 68–76. doi: 10.1007/978-981-10-6451-7_9.

Tabari, H. (2020). Climate change impact on flood and extreme precipitation increases with water availability. *Scientific Reports*, 10 (1), 1–10.

Taheri, M., & Ahmad, L. (2012). Application of Remote Sensing and GIS in Preparing Land Cover and Land Use Information Layers for MPSIAC Erosion Model, First National Conference on Strategies for Achieving Sustainable Development (Agriculture, Natural Resources and Environment), Tehran.

Tang, Z., Zhang, H., Yi, S., & Xiao, Y. (2018). Assessment of flood susceptible areas using spatially explicit, probabilistic multi-criteria decision analysis. *Journal of Hydrology*, 558, 144-158, https://doi.org/10.1016/j.jhydrol.2018.01.033.

Tehrany, M. S., & Kumar, L. (2018). application of a Dempster–Shafer-based evidential belief function in flood susceptibility mapping and comparison with frequency ratio and logistic regression methods. *Environmental Earth Sciences*, 77, 490.

Tehrany, M. S., Kumar, L., & Shabani, F. (2019). A novel GIS-based ensemble technique for flood susceptibility mapping using evidential belief function and support vector machine: Brisbane, Australia. PeerJ 7: e7653.

Tehrany, M. S., Kumar, L., Neamah Jebur, M., & Shabani, F. (2019). Evaluating the application of the statistical index method in flood susceptibility mapping and its comparison with frequency ratio and logistic regression methods. *Geomat Nat Haz Risk*, 10 (1), 79–101.

Tien Bui, D., Bui, Q.T., Nguyen, Q.P., Pradhan, B., Nampak, H., & Trinh, P.T. (2017). A hybrid artificial intelligence approach using GIS-based neural-fuzzy inference system and particle swarm optimization for forest fire susceptibility modeling at a tropical area. *Agricultural and Forest Meteorology*, 233, 32-44.

Upretia, P., & Ojha, C. (2022). Development and performance evaluation of SCS-CN based hybrid model. *Water Science & Technology*. 85. 2479 doi: 10.2166/wst.2022.145.

Wang, L. J., Guo, M., Sawada, K., Lin, J., & Zhang, J. (2015). Landslide susceptibility mapping in MizunamiCity, Japan: A comparison between logistic regressionbivariate statistical analysis and multivariate adaptiveRegression spline models. *Catena*, 135, 271-282.

Wang, Y., Fang, Z., Hong, H., & Peng, L.

(2020). Flood susceptibility mapping using convolutional neural network frameworks. *J. Hydrol*, 582, 124482.

Wang, Y., Hong, H., Chen, W., Li, S., Pamučar, D., Gigović, L., Drobnjak, S., Tien Bui, D., & Duan, H. (2019.) A hybrid GIS multi-criteria decision-making method for flood susceptibility mapping at Shangyou, China. *Remote Sens*, 11 (1), 62.

Wang, Y., Hong, H., Chen, W., Li, S., Panahi, M., Khosravi, K., Shirzadi, A., Shahabi, H., Panahi, S., & Costache, R. (2019). Flood susceptibility mapping in Dingnan County (China) using adaptive neuro-fuzzy inference system with biogeography based optimization and imperialistic competitive algorithm. *J. Environ. Manage*, 247, 712–729.

Winsemius, H. C., Van Beek, L. P. H., Jongman, B., Ward, P. J., & Bouwman, A. (2013). A framework for global river flood risk assessments. *Hydrol. Earth Syst. Sci*, 17, 1871–1892. doi: 10.5194/hess-17-1871-2013.

Wubalem, A., Tesfaw, G., Dawit, Z., Getahun, B., Mekuria, T., & Jothimani, M. (2021). Comparison of statistical and analytical hierarchy process methods on flood susceptibility mapping: In a case study of the Lake Tana sub-basin in northwestern Ethiopia. *Open Geosciences*, 13, 1668–1688.

Xie, H., Dong, J., Shen, Z., Chen, L., Lai, X., Qiu, J., & Chen, X. (2019). Intra-and inter-event characteristics and controlling factors of agricultural nonpoint source pollution under different types of rainfall-runoff events. *Catena*, 182,104105.

Xu, Q., Shi, Y., Bamber, L., Ouyang, Ch., & Xiang Zhu, X. (2024). Large-scale flood modeling and forecasting with FloodCast, *Water Research*, 264, 122162. https://doi.org/10.1016/j.watres.2024.122162

Yamazaki, D., Kanae, S., Kim, H., & Oki, T. (2011). A physically based description of floodplain inundation dynamics in a global river routing model. *Water Resour. Res*, 47:W04501. doi: 10.1029/2010WR009726.

Zhao, G., Pang, B., Xu, Z., Yue, J., & Tu, T. (2018). Mapping flood susceptibility in mountainous areas on a national scale in China. *Sci Total Environ*, 615,1133–42.

Zhao, R. J., Liu, X. R., & Singh, V. P. (1995). The Xinanjiang model. Comput. Models Watershed Hydrol 135, 371–381.